Research Paper
Computational Methods for Differential Equations
http://cmde.tabrizu.ac.ir
Vol. *, No. *, *, pp. 1-14
DOI:10.22034/cmde.2026.70603.3518

Application of IEFG method for optimal control of elliptic variational inequality

Mahmood Khaksar-e Oshagh*
Department of Mathematics Education, Farhangian University, P. O. Box 14665-889, Tehran, Iran.

Abstract

This paper presents the Interpolating Element-Free Galerkin (IEFG) method for the numerical solution of an optimal control problem constrained by an elliptic variational inequality. The proposed approach is an indirect approach: the optimality system is derived via a Lagrangian formulation, leading to mixed complementarity conditions that are solved numerically using a meshfree scheme based on moving least squares approximation with Kronecker-delta property. The method is mesh-free and can be used with irregular node distributions and even in irregular domains. To verify the reliability of the proposed scheme, its convergence properties are also numerically investigated and several numerical tests for the optimal control problem are carried out using the developed method. The computational results illustrate the accuracy and robustness of the approach.

Keywords. Optimal control of variational inequalities, Elliptic variational inequality, Interpolating element-free Galerkin (IEFG) method, Meshfree methods.

2010 Mathematics Subject Classification. 65K15, 35J86, 49J21.

1. Introduction

The mathematical theory of elliptic variational inequalities was initially developed to deal with equilibrium problems. However, this type of inequality appears in the description of many scientific phenomena. Mostly, contact problems such as the obstacle problem [4] and the Signorini problem [7] can be explained as an inequality involving an elliptic function that holds for all possible values of a given variable, usually belonging to a convex set. This is an elliptic variational inequality [12, 28].

An optimal control problem is a mathematical optimization problem that seeks to find a control function that minimizes (or maximizes) a performance criterion, subject to the dynamics of a system described by differential equations (or variational inequalities) and possibly additional constraints. Formally, consider a system whose state y evolves according to a differential equation (or variational inequality) parameterized by a control function u. The goal is to find u that minimizes a cost functional of the form [22]:

$$\mathcal{F}[y,u] = \int_\Omega L(\mathbf{x}, y(\mathbf{x}), u(\mathbf{x}))\, d\mathbf{x}.$$

The state y is linked to the control u through a state equation (e.g., a partial differential equation or a variational inequality). The problem may also include constraints on the state or control, such as $y \le z$ (obstacle constraint), box constraints on u, or boundary conditions.

Optimal control problems arise in a wide range of scientific and engineering disciplines. Classical examples include trajectory optimization (finding the path of a rocket that minimizes fuel consumption), structural design (determining the shape of a beam that minimizes deformation under load), economics (optimizing investment strategies over time), and biomedical engineering (designing optimal drug delivery protocols). For recent developments in numerical methods for optimal control problems, see [10, 15, 22, 23, 29, 31].

Received: 07 December 2025; Accepted: 22 August 2026.
∗ Corresponding author. Email: m.khaksar@cfu.ac.ir.

More specifically, there are many examples of optimal control problems governed by variational inequalities. In contact mechanics, these problems model the optimal shaping of elastic bodies in contact with rigid obstacles. In financial mathematics, they appear in optimal stopping problems such as American option pricing. In biomedical engineering, they are used for optimal therapy design in cancer treatment. For a comprehensive review, see [5, 12, 14].

Most of these optimal control problems do not have analytical solutions. Therefore, the development of efficient numerical techniques for treating such problems has attracted considerable attention in recent years. Although the majority of classical approaches rely on finite difference and finite element schemes [18], the advent of meshless methods has introduced a promising alternative for researchers working in this area.

Meshfree strategies avoid the need for a predefined mesh over the computational domain and can be applied on both structured and unstructured node distributions. These methods typically offer simpler implementation procedures and exhibit a natural capability for extension to higher-dimensional settings.

The element-free Galerkin (EFG) method is formulated on a global weak form, where the moving least-squares (MLS) approximation is used to construct both trial and test functions. It was initially proposed by Belytschko et al. in 1994 [6] to solve boundary value problems. In this technique, the weak form integral equation of the problem is extracted and applied on subdomains that are not necessarily regular. Then, the shape functions of the moving least squares method are used as the test and trial functions in the Galerkin method to solve this weak form. Using an appropriate numerical integration scheme, the weak formulation is converted into a system of algebraic equations, whose solution provides the numerical approximation to the desired field variables [13].

However, a known drawback of MLS basis functions is that they do not satisfy the Kronecker-delta property, which prevents the direct imposition of essential boundary conditions. To address this difficulty, the interpolating moving least-squares (IMLS) approximation was introduced, providing basis functions that do satisfy the Kronecker-delta condition. When MLS functions are replaced by their interpolating counterparts, the resulting scheme is commonly known as the interpolating element-free Galerkin (IEFG) method [2]. In this paper, we focus on presenting a mesh-free numerical method to solve the optimal control problem of an elliptic variational inequality. To this end, a combination of the IEFG method with an efficient algorithm for solving this problem, known as the active set algorithm, has been employed. The main objective of this paper is to demonstrate that the IEFG method, a globally weak-form method, can be effectively applied to optimal control of variational inequalities, similar to its successful applications in solving PDEs.

Recent developments in meshfree methods for optimal control problems include the works of [3, 9, 26]. The interpolating moving least squares approach has been extended to various settings in [8, 25]. For optimal control of variational inequalities, the active-set strategy has been successfully combined with finite elements [14, 16] and wavelet methods [19]. The present work contributes to this literature by introducing a meshfree IEFG framework that combines the geometric flexibility of meshfree methods with the theoretical guarantees of the active-set approach.

1.1. **Notation and Function Spaces.** Throughout this paper, we denote by $\Omega \subset \mathbb{R}^2$ a bounded domain with Lipschitz boundary $\Gamma = \partial\Omega$. The following function spaces are used:

- $L^2(\Omega)$: the space of square-integrable functions with norm $\|v\|_{L^2} = (\int_\Omega v^2 d\mathbf{x})^{1/2}$.
- $H^1(\Omega)$: the Sobolev space of functions in $L^2(\Omega)$ with first-order weak derivatives in $L^2(\Omega)$.
- $H_0^1(\Omega)$: the subspace of $H^1(\Omega)$ with vanishing trace on Γ.
- $H^{-1}(\Omega)$: the dual space of $H_0^1(\Omega)$.

The inner product on $L^2(\Omega)$ is denoted by $(\cdot,\cdot)$ and the bilinear form $b(\cdot,\cdot) : H_0^1(\Omega) \times H_0^1(\Omega) \to \mathbb{R}$ is defined as $b(y,v) = \int_\Omega \nabla y \cdot \nabla v \, d\mathbf{x}$.

2. Problem Statement and Its Optimality Conditions

Let $\mathcal{W}$ be a real Hilbert space with dual space $\mathcal{W}^*$ and inner product $(\cdot,\cdot)_{\mathcal{W}}$. Let $b(\cdot,\cdot)$ be a bounded and continuous bilinear form on $\mathcal{W} \times \mathcal{W}$ and K be a closed convex subset of $\mathcal{W}$. If b is coercive then there exists a linear operator associated with the bilinear form b, i.e., $b(v,s) = (\mathcal{B}v, s)_{\mathcal{W}}$. Let $\mathcal{U}_{ad}$ be a set of admissible control functions. By considering y as the state function belonging to $\mathcal{W}$ and $u \in \mathcal{U}_{ad}$ as the control function, an optimal control problem governed by an elliptic variational inequality has the following form:

$$\begin{aligned} &\text{Min } \mathcal{F}[y,u] \\ &\text{over } (y,u) \in \mathcal{W} \times \mathcal{U}_{ad} \\ &\text{s. t. } b(y, y-w) \le (g+u, y-w)_{\mathcal{W}}, \quad \forall w \in K \subset \mathcal{W} \end{aligned} \tag{2.1}$$

where $\mathcal{F}$ is an objective functional and $g \in \mathcal{U}_{ad}$ is a known function.

2.1. **The Specific Problem Considered in This Paper.** The above problem is the general form. In more practical cases, we consider the state function belongs to $H_0^1(\Omega)$ where Ω is the computational domain with variable $\mathbf{x}$. The set of admissible control is $L^2(\Omega)$. Also, $y_g \in H_0^1(\Omega)$ is the target function to which the state function should be as close as possible. Now, the objective functional $\mathcal{F}$ is usually considered as follows [17]

$$\mathcal{F}[y,u] := \mathcal{T}[y] + \omega\mathcal{S}[u] = \frac{1}{2}\int_\Omega (y-y_g)^2 d\mathbf{x} + \frac{\omega}{2}\int_\Omega u^2 d\mathbf{x}.$$

From now on, by defining the elliptic form $b(\cdot,\cdot) = (\nabla\cdot, \nabla\cdot)$, we consider an elliptic variational inequality

$$(\nabla y, \nabla(y-w)) \le (g+u, y-w), \quad \forall w \in K_z, \tag{2.2}$$

$$K_z = \{y \in H_0^1(\Omega) \mid y(\mathbf{x}) \le z(\mathbf{x}) \text{ a.e. in } \Omega\}, \tag{2.3}$$

as the constraint of the optimal control problem (2.1). Thus, the optimal control problem considered in this paper is formulated as follows, and for convenience, we will refer to it as (P) throughout the rest of the paper.

$$\begin{aligned} &\text{Min } \mathcal{F}[y,u] = \mathcal{T}[y] + \omega\mathcal{S}[u] \\ &\text{over } (y,u) \in H_0^1(\Omega) \times L^2(\Omega) \\ &\text{s. t. } (\nabla y, \nabla(y-w)) \le (g+u, y-w), \quad \forall w \in K_z. \end{aligned} \tag{P}$$

2.2. **Optimality Conditions for the Regularized Problem.** Now, we focus on deriving the optimality conditions for the optimal control problem (P) using the method described in [14]. This approach is based on introducing appropriate Lagrange multipliers for the problem.

First, we need the strong form of problem (2.2)-(2.3). It is worthy to note that if $y \in H^2(\Omega)$ is a solution of the elliptic variational inequality (2.2)-(2.3) then it satisfies the following complementarity problem [19]

$$-\Delta y \le g + u, \tag{2.4}$$

$$y \le z, \tag{2.5}$$

$$(\Delta y + g + u)(y - z) = 0. \tag{2.6}$$

The latter problem is the strong form of the considered variational inequality.

The complementarity conditions indicate that the analytical solution of (2.2)-(2.3) divides the domain Ω into two parts, which are called the active and inactive sets, respectively [11]:

$$\mathcal{A} := \{\mathbf{x} \in \Omega \mid y(\mathbf{x}) = z(\mathbf{x}) \ \wedge \ -\Delta y(\mathbf{x}) < g(\mathbf{x}) + u(\mathbf{x})\}, \tag{2.7}$$

$$\mathcal{N} := \{\mathbf{x} \in \Omega \mid -\Delta y(\mathbf{x}) = g(\mathbf{x}) + u(\mathbf{x}) \ \wedge \ y(\mathbf{x}) < z(\mathbf{x})\}. \tag{2.8}$$

Note that the boundary between these parts is unknown and emerges as part of the solution. Also, the non-smoothness of state and control functions along this unknown free boundary is expected.

Introducing the Lagrange multiplier λ allows the complementarity system (2.4)–(2.6) to be written in the equivalent form [16]

$$-\Delta y + \lambda = u + g, \tag{2.9}$$

$$\lambda = \max\{0, \lambda + \eta(y - z)\}, \tag{2.10}$$

where η is a positive real constant. Although this reformulation removes the explicit inequality constraints, the term $\max\{\cdot\}$ still introduces a non-differentiability, meaning that the optimal control problem (P) remains non-regular and requires a suitable smoothing strategy.

Following [19], we employ the smooth approximation

$$\max{}_c\{0,x\} = \begin{cases} 0, & x \le \frac{-1}{2c}, \\ \frac{c}{2}x^2 + \frac{1}{2}x + \frac{1}{8c}, & \frac{-1}{2c} \le x \le \frac{1}{2c}, \\ x, & x \ge \frac{1}{2c}. \end{cases}$$

of the function $\max\{\cdot\}$, which is a $C^1(\mathbb{R})$ function with derivative

$$D_c(x) = \begin{cases} 0, & x \le \frac{-1}{2c}, \\ cx + 0.5, & \frac{-1}{2c} \le x \le \frac{1}{2c}, \\ 1, & x \ge \frac{1}{2c}. \end{cases}$$

Thus, we can define the regularized version of (P) as

$$\begin{aligned} \text{Min} \quad & \mathcal{F}[y,u] \\ \text{s.t.} \quad & -\Delta y + \lambda = u + g, \\ & \lambda = \max{}_c\{0, \lambda + \eta(y-z)\}. \end{aligned} \tag{Pc}$$

The regularized problem (Pc) admits a unique solution (y_c, u_c), and as $c \to \infty$ these solutions possess weak cluster points (y^*, u^*) that solve the original optimal control problem (P).

To derive the first-order optimality conditions for (Pc), by considering α_c and β_c as Lagrange multipliers [10], the Lagrangian functional is defined as

$$\mathcal{L}[y,u,\lambda,\alpha,\beta] = \mathcal{F}[y,u] - (\Delta y - \lambda + u + g, \alpha_c) + (\max{}_c\{0, \lambda + \eta(y-z)\} - \lambda, \beta_c).$$

Taking variations with respect to all variables yields

$$\begin{aligned} & -\Delta y + \lambda - u - g = 0, \\ & \lambda - \max{}_c\{0, \lambda + \eta(y-z)\} = 0, \\ & y - y_g - \Delta\alpha_c + \eta D_c(\lambda + \eta(y-z))\beta_c = 0, \\ & \alpha_c + (D_c(\lambda + \eta(y-z)) - 1)\beta_c = 0, \\ & \omega u - \alpha_c = 0. \end{aligned}$$

Let α^* and β^* denote weak limits of (α_c) and (β_c), respectively. Then, according to [14], they satisfy

$$\begin{aligned} & -\Delta y^* + \lambda^* - u^* - g = 0, \\ & \lambda^* - \max\{0, \lambda^* + \eta(y^* - z)\} = 0, \\ & y^* - y_g - \Delta\alpha^* + \eta\chi_{\mathcal{A}}(\lambda^* + \eta(y^* - z))\beta^* = 0, \\ & \alpha^* + (\chi_{\mathcal{A}}(\lambda^* + \eta(y^* - z)) - 1)\beta^* = 0, \\ & \omega u^* - \alpha^* = 0, \end{aligned}$$

where $\chi_{\mathcal{A}}$ represents the indicator function of the set $\mathcal{A}$. Using the definition of the indicator function $\chi_{\mathcal{A}}$ and eliminating the auxiliary variables, the optimality conditions for the original problem (P) reduce to [14]

$$\lambda - \Delta y - u - g = 0, \tag{2.11a}$$
$$\lambda - \max\{0, \lambda + \eta(y-z))\} = 0, \tag{2.11b}$$
$$y - y_g - \omega\Delta u = 0, \quad \text{in } \mathcal{N}, \tag{2.11c}$$
$$u = 0, \quad \text{in } \mathcal{A}. \tag{2.11d}$$

The numerical implementation presented in the next section is based on the optimality system (2.11).

3. Interpolating Element-Free Galerkin Method

Meshfree methods approximate solutions using a set of scattered nodes without requiring a structured mesh. The interpolating element-free Galerkin (IEFG) method uses IMLS shape functions that satisfy the Kronecker-delta property, enabling direct imposition of Dirichlet boundary conditions. In this section, we introduce the element-free Galerkin (EFG) and interpolating element-free Galerkin (IEFG) methods. To do this, it is necessary to first introduce the moving least squares (MLS) [27] and the interpolating moving least squares (IMLS) shape functions.

Let $\Xi_I = \{\mathbf{x}_l\}_{l=1}^{N_I}$ and $\Xi_b = \{\mathbf{x}_l\}_{l=1}^{N_b}$ be the sets of selected nodes in the computational domain Ω and on its boundary Γ, respectively. Their union is $\Xi = \{\mathbf{x}_l\}_{l=1}^{N}$ where $N = N_I + N_b$.

3.1. Moving Least Squares (MLS) Shape Functions.

Given a set of known function values $\mathbf{f} = \{f_l = f(\mathbf{x}_l)\}_{l=1}^{N}$ defined on the point set Ξ, a local approximation $\hat{f}$ at a point $\mathbf{x}$ can be constructed in the form:

$$\hat{f}(\mathbf{x}, \bar{\mathbf{x}}) := \mathbf{\Phi}^t(\bar{\mathbf{x}}) \cdot \mathbf{a}(\mathbf{x}) = \sum_{l=1}^{M} a_l(\mathbf{x})\, \phi_l(\bar{\mathbf{x}}), \tag{3.1}$$

where $\{\phi_l\}$ represent spatial basis functions, typically selected as monomials in multiple variables.

In this formulation, $\bar{\mathbf{x}} \in \Xi$ denotes a point located within the local influence domain of the node $\mathbf{x}_i$. The extent of this domain is governed by a compactly supported radial weight function $w_i(\mathbf{x})$.

Within the moving least squares (MLS) framework, the unknown coefficients $\{a_l(\mathbf{x})\}$ are determined through the minimization of the following weighted residual functional:

$$\min_{\{a_k(\mathbf{x})\}} \sum_{l=1}^{N} w_l(\mathbf{x}) \left[\sum_{k=1}^{M} a_k(\mathbf{x})\, \phi_k(\mathbf{x}_l) - f_l \right]^2. \tag{3.2}$$

The minimization of the functional (3.2) with respect to the coefficient vector $\mathbf{a}(\mathbf{x})$ requires the satisfaction of the stationary condition derived from the first variation. This yields the following linear system [25]:

$$\left(\mathbf{A}^t\, \mathbf{Q}(\mathbf{x})\, \mathbf{A}\right) \mathbf{a}(\mathbf{x}) = \mathbf{A}^t\, \mathbf{Q}(\mathbf{x})\, \mathbf{f}, \tag{3.3}$$

wherein $\mathbf{A}$ denotes an $N \times M$ matrix with entries $A_{nm} = \phi_m(\mathbf{x}_n)$ for $n = 1, \dots, N$ and $m = 1, \dots, M$. Furthermore, $\mathbf{Q}(\mathbf{x})$ represents a diagonal weighting matrix defined by $\mathbf{Q}_{ii}(\mathbf{x}) = w_i(\mathbf{x})$.

Upon solving (3.3) for $\mathbf{a}(\mathbf{x})$ and inserting the result into the local approximation (3.1), the expression becomes:

$$\hat{f}(\mathbf{x}, \bar{\mathbf{x}}) := \mathbf{\Phi}^t(\bar{\mathbf{x}}) \cdot \left(\mathbf{A}^t\, \mathbf{Q}(\mathbf{x})\, \mathbf{A}\right)^{-1} \mathbf{A}^t\, \mathbf{Q}(\mathbf{x})\, \mathbf{f}. \tag{3.4}$$

The MLS shape functions are formally defined as the row vector

$$\bar{\mathbf{S}}(\mathbf{x}) = \left(\bar{S}_1(\mathbf{x}), \dots, \bar{S}_N(\mathbf{x})\right) = \mathbf{\Phi}^t(\mathbf{x}) \left(\mathbf{A}^t\, \mathbf{Q}(\mathbf{x})\, \mathbf{A}\right)^{-1} \mathbf{A}^t\, \mathbf{Q}(\mathbf{x}). \tag{3.5}$$

Consequently, the moving least squares approximation (3.4) of the function f admits the compact representation:

$$\hat{f}(\mathbf{x}) = \bar{\mathbf{S}}(\mathbf{x}) \cdot \mathbf{f} = \sum_{l=1}^{N} \bar{S}_l(\mathbf{x})\, f_l. \tag{3.6}$$

When the MLS shape functions are employed as both trial and test functions within a conventional Galerkin formulation, the resulting numerical scheme is termed the element-free Galerkin (EFG) method. However, since these functions do not have the Kronecker-delta property, the resulting approximation does not possess the interpolation property at the desired points, and Dirichlet boundary conditions cannot be imposed directly.

3.2. Interpolating Moving Least Squares (IMLS) Shape Functions.

To enforce interpolation properties, a singular radial basis function is introduced as the weight function from this point onward [1]:

$$w_l(\mathbf{x}) = \begin{cases} \|\mathbf{x} - \mathbf{x}_l\|^{-\gamma}, & \|\mathbf{x} - \mathbf{x}_l\| \le r, \\ 0, & \text{Otherwise.} \end{cases} \tag{3.7}$$

Equipping the space with the discrete inner product $(f,g)_{\mathbf{w}} = \sum_{l=1}^{N} w_l(\mathbf{x})\, f_l\, g_l$, induces the corresponding norm $\|f\|_{\mathbf{w}} = \sqrt{(f,f)_{\mathbf{w}}}$.

Assuming $\phi_1(\mathbf{x}) \equiv 1$, the first orthonormal basis element is constructed as

$$B_{1,\mathbf{x}}(\mathbf{x}) = \frac{\phi(\mathbf{x})}{\|\phi_1\|_{\mathbf{w}}} = \frac{1}{\sqrt{\sum_{l=1}^{N} w_l(\mathbf{x})}}. \tag{3.8}$$

Applying the Gram–Schmidt orthogonalization procedure to the set $\{\phi_2, \dots, \phi_M\}$ relative to $B_{1,\mathbf{x}}$ yields, for $k = 2, \dots, M$,

$$B_{k,\mathbf{x}}(\mathbf{x}) = \phi_k(\mathbf{x}) - (\phi_k, B_{1,\mathbf{x}})_{\mathbf{w}}\, B_{1,\mathbf{x}}(\mathbf{x}) = \phi_k(\mathbf{x}) - \frac{\sum_{l=1}^{N} \phi_k(\mathbf{x}_l) w_l(\mathbf{x})}{\sum_{l=1}^{N} w_l(\mathbf{x})}. \tag{3.9}$$

Considering $\mathbf{D}(\mathbf{x}) = [B_{k,\mathbf{x}}(\mathbf{x}_l)]_{\substack{l=1,\dots,N\\ k=2,\dots,M}}$ and $\mathbf{B}^t(\mathbf{x}) = [B_{k,\mathbf{x}}(\mathbf{x})]_{k=1,\dots,M}$ and defining the constituent matrices $\mathbf{L}(\mathbf{x}) = \mathbf{D}^t(\mathbf{x})\,\mathbf{Q}(\mathbf{x})$ and $\mathbf{R}(\mathbf{x}) = \mathbf{L}(\mathbf{x})\,\mathbf{D}(\mathbf{x})$, the orthogonality condition between $B_{1,\mathbf{x}}$ and $\{B_{k,\mathbf{x}}\}_{k=2}^{M}$ leads to the following interpolating approximation [1]:

$$f(\mathbf{x}) \simeq f_h(\mathbf{x}) = \mathbf{v}^t(\mathbf{x})\,\mathbf{f} + \mathbf{B}^t(\mathbf{x})\,\mathbf{R}^{-1}(\mathbf{x})\,\mathbf{L}(\mathbf{x})\,\mathbf{f}, \tag{3.10}$$

where $\mathbf{v}^t(\mathbf{x}) = [v_l(\mathbf{x})]_{l=1,\dots,N}$ with

$$v_l(\mathbf{x}) := \frac{w_l(\mathbf{x})}{\sum_{l=1}^{N} w_l(\mathbf{x})}.$$

The approximation (3.10) motivates the definition of the interpolating moving least squares (IMLS) shape functions:

$$\mathbf{S}(\mathbf{x}) := \big(S_1(\mathbf{x}), \dots, S_N(\mathbf{x})\big) = \mathbf{v}^t(\mathbf{x}) + \mathbf{B}^t(\mathbf{x})\,\mathbf{R}^{-1}(\mathbf{x})\,\mathbf{L}(\mathbf{x}). \tag{3.11}$$

Consequently, (3.10) admits the compact form:

$$f_h(\mathbf{x}) = \mathbf{S}(\mathbf{x})\,\mathbf{f} = \sum_{k=1}^{N} S_k(\mathbf{x})\, f_k. \tag{3.12}$$

Property 1. *The IMLS shape functions defined in (3.11) satisfy $S_j(\mathbf{x}_i) = \delta_{ij}$ for all $\mathbf{x}_i, \mathbf{x}_j \in \Xi$, where δ_{ij} is the Kronecker delta. This property enables the direct imposition of essential boundary conditions in the IEFG method [1].*

These IMLS shape functions are now suitable for adoption as both trial and test functions in a conventional Galerkin weak formulation. Their Kronecker-delta property facilitates the direct and straightforward imposition of essential boundary conditions. The resulting numerical scheme is referred to as the interpolating element-free Galerkin (IEFG) method.

Theorem 3.1. *Let $y \in H^{p+1}(\Omega)$ with $p \geq 1$. Let y_h be the IMLS approximation defined in (3.12) using a basis of degree p and a nodal fill distance $h = \max_i \min_{j\neq i} \|\mathbf{x}_i - \mathbf{x}_j\|$. Then there exists a constant $C > 0$, independent of h, such that*

$$\|y - y_h\|_{L^2} \leq C h^{p+1} \|y\|_{H^{p+1}}, \qquad \|\nabla(y - y_h)\|_{L^2} \leq C h^{p} \|y\|_{H^{p+1}}.$$

For the proof, see [24, 30].

4. Implementation

It should be noted that while the following iteration, named the active set, is conceptually independent of the discretization, the standard active-set update formulas have been adapted and rewritten specifically for the IMLS-based spatial approximation. Therefore, the name IEFG reflects the fact that the entire solution process, including the active-set update, is carried out within the interpolating element-free Galerkin framework.

Solving (2.11a) for the Lagrange multiplier λ and inserting the result into Equation (2.11b) produces the condition:

$$\Delta y + u + g = \max\{0,\ \Delta y + u + g + \eta\,(y - z)\}\,.$$

This reformulation naturally motivates an iterative algorithm for the coupled system (2.11a)–(2.11b). The scheme updates the solution as follows:

$$\Delta y^{(k+1)} + u^{(k+1)} + g = \max\left\{0,\ \Delta y^{(k)} + u^{(k)} + g + \eta\left(y^{(k+1)} - z\right)\right\}. \tag{4.1}$$

Thus, to construct a viable numerical scheme for the optimal control problem (P), we employ the iterative equation (4.1) together with the optimality conditions (2.11c)-(2.11d). The proposed algorithm operates by iteratively identifying active and inactive point sets, imposing the corresponding optimality conditions on each set, and subsequently refining this classification.

Let $\left(y^{(k)}, u^{(k)}, \lambda^{(k)}\right)$ denote the numerical approximations obtained at the k-th iteration. Utilizing the partition defined in (2.7)–(2.8) and the Lagrangian formulation (2.10), the updated active and inactive sets are determined by the following criteria:

$$\mathcal{A}^{(k+1)} = \left\{\mathbf{x} \in \Omega \;\middle|\; \lambda^{(k)}(\mathbf{x}) + \eta\left(y^{(k)}(\mathbf{x}) - z(\mathbf{x})\right) > 0\right\}, \tag{4.2}$$

$$\mathcal{N}^{(k+1)} = \left\{\mathbf{x} \in \Omega \;\middle|\; \lambda^{(k)}(\mathbf{x}) + \eta\left(y^{(k)}(\mathbf{x}) - z(\mathbf{x})\right) \le 0\right\}. \tag{4.3}$$

Taking into account relations (2.11d) and (4.2), the update rule at a point $\mathbf{x} \in \mathcal{A}^{(k+1)}$ is governed by:

$$\Delta y^{(k+1)}(\mathbf{x}) = \Delta y^{(k)}(\mathbf{x}) + u^{(k)}(\mathbf{x}) + \eta\left(y^{(k+1)}(\mathbf{x}) - z(\mathbf{x})\right). \tag{4.4}$$

Conversely, for points in the inactive region $\mathbf{x} \in \mathcal{N}^{(k+1)}$, Equation (2.11c) together with the condition $\lambda^{(k+1)}(\mathbf{x}) = 0$ leads to the system:

$$-\Delta y^{(k+1)}(\mathbf{x}) - u^{(k+1)}(\mathbf{x}) = g(\mathbf{x}), \tag{4.5}$$

$$y^{(k+1)}(\mathbf{x}) - y_d(\mathbf{x}) - \omega\,\Delta u^{(k+1)}(\mathbf{x}) = 0. \tag{4.6}$$

The state and control functions are approximated using the IMLS representation given in (3.12):

$$y^{(k+1)}(\mathbf{x}) \approx \hat{y}^{(k+1)}(\mathbf{x}) = \mathbf{S}(\mathbf{x}) \cdot \mathbf{y}^{(k+1)},$$
$$u^{(k+1)}(\mathbf{x}) \approx \hat{u}^{(k+1)}(\mathbf{x}) = \mathbf{S}(\mathbf{x}) \cdot \mathbf{u}^{(k+1)}.$$

Now, to derive the weak formulation, we start from the strong form of the equations on each subdomain. Multiplying (4.5) by a test function $v \in H_0^1(\Omega)$ and integrating over $\mathcal{N}^{(k+1)}$ and applying the divergence theorem (Green's formula) to the first term gives:

$$\int_{\mathcal{N}^{(k+1)}} \nabla y^{(k+1)} \cdot \nabla v\, dx - \int_{\Gamma} (\nabla y^{(k+1)} \cdot n) v\, ds - \int_{\mathcal{N}^{(k+1)}} u^{(k+1)} v\, dx = \int_{\mathcal{N}^{(k+1)}} g v\, dx. \tag{4.7}$$

where Γ is the obtained boundary between active and in active sets. In the same manner, multiplying by the same test function v and integrating over $\mathcal{A}^{(k+1)}$ from (4.4) yields:

$$\int_{\mathcal{A}^{(k+1)}} \nabla y^{(k+1)} \cdot \nabla v\, dx + \int_{\Gamma} (\nabla y^{(k+1)} \cdot n) v\, ds + \eta \int_{\mathcal{A}^{(k+1)}} y^{(k+1)} v\, dx = \int_{\mathcal{A}^{(k+1)}} (-\Delta y^{(k)} - u^{(k)} + \eta z) v\, dx. \tag{4.8}$$

Now, adding Equations (4.7) and (4.8), the boundary integrals on Γ cancel out, yielding the unified weak form over the entire domain Ω:

$$\int_{\Omega} \nabla y^{(k+1)} \cdot \nabla v\, dx + \eta \int_{\mathcal{A}^{(k+1)}} y^{(k+1)} v\, dx - \int_{\mathcal{N}^{(k+1)}} u^{(k+1)} v\, dx = \int_{\Omega} f v\, dx, \tag{4.9}$$

where the right-hand side function f is defined piecewise as:

$$f(\mathbf{x}) := \begin{cases} -\Delta y^{(k)}(\mathbf{x}) - u^{(k)}(\mathbf{x}) + \eta\, z(\mathbf{x}), & \mathbf{x} \in \mathcal{A}^{(k+1)}, \\ g(\mathbf{x}), & \mathbf{x} \in \mathcal{N}^{(k+1)}. \end{cases}$$

Moreover, multiplying (4.6) by v and integrating on $\mathcal{N}^{(k+1)}$ and using Green formula with vanishing u on the boundary Γ gives:

$$\omega \int_{\mathcal{N}^{(k+1)}} \nabla u^{(k+1)} \cdot \nabla v \, d\mathbf{x} + \int_{\mathcal{N}^{(k+1)}} y^{(k+1)} v \, d\mathbf{x} = \int_{\mathcal{N}^{(k+1)}} y_d v \, d\mathbf{x}. \tag{4.10}$$

Employing the IMLS shape functions from (3.12) as test functions ($v = S_i$) on (4.9) and (4.10) yields the discretized linear system:

$$(\mathbf{H} + \eta \mathbf{L})\, \hat{\mathbf{y}} - \mathbf{M}\, \hat{\mathbf{u}} = \mathbf{F}, \tag{4.11}$$

$$\mathbf{M}\, \hat{\mathbf{y}} + \omega\, \mathbf{H}\, \hat{\mathbf{u}} = \mathbf{G}, \tag{4.12}$$

where the matrices appearing in the above equations are assembled from the following integrals:

$$\mathbf{H}_{ij} = \int_{\Omega} \nabla S_i(\mathbf{x}) \cdot \nabla S_j(\mathbf{x}) \, d\mathbf{x}, \tag{4.13}$$

$$\mathbf{L}_{ij} = \int_{\mathcal{A}^{(k+1)}} S_i(\mathbf{x}) S_j(\mathbf{x}) \, d\mathbf{x}, \tag{4.14}$$

$$\mathbf{M}_{ij} = \int_{\mathcal{N}^{(k+1)}} S_i(\mathbf{x}) S_j(\mathbf{x}) \, d\mathbf{x}. \tag{4.15}$$

Furthermore, the load vectors on the right-hand side are given by:

$$\mathbf{F}_i = \int_{\Omega} f(\mathbf{x}) S_i(\mathbf{x}) \, d\mathbf{x}, \tag{4.16}$$

$$\mathbf{G}_i = \int_{\mathcal{N}^{(k+1)}} y_d(\mathbf{x}) S_i(\mathbf{x}) \, d\mathbf{x}. \tag{4.17}$$

Since the optimality condition (2.11d) imposes $u = 0$ on the active set $\mathcal{A}$, and the boundary $\partial\Omega$ is typically contained in $\mathcal{A}$ (or its closure), the control u satisfies homogeneous Dirichlet boundary conditions. These are imposed directly through the IMLS shape functions, which vanish on the boundary nodes due to the Kronecker-delta property.

Algorithm 1: IEFG algorithm for optimal control of elliptic variational inequality.

Input: Initial guess $y^{(0)}$, $u^{(0)}$, $\lambda^{(0)}$; parameters η and $K_{\max}$.
Output: Optimal state y^*, control u^*, and Lagrange multiplier λ^*.
$k \leftarrow 0$;
repeat
  Update active/inactive sets using (4.2)-(4.3):
  $\mathcal{A}^{(k+1)} = \{\mathbf{x} \mid \lambda^{(k)} + \eta(y^{(k)} - z) > 0\}$,
  $\mathcal{N}^{(k+1)} = \Xi \setminus \mathcal{A}^{(k+1)}$;
  Assemble matrices $\mathbf{H}, \mathbf{L}^{(k+1)}, \mathbf{M}^{(k+1)}$ using IMLS shape functions from (4.13)-(4.15);
  Assemble the right-hand side vectors $\mathbf{F}^{(k+1)}$ and $\mathbf{G}^{(k+1)}$ from (4.16)-(4.17);
  Solve the linear system (4.11)-(4.12) for $\mathbf{y}^{(k+1)}$ and $\mathbf{u}^{(k+1)}$:

$$\begin{pmatrix} \mathbf{H} + \eta \mathbf{L}^{(k+1)} & -\mathbf{M}^{(k+1)} \\ \mathbf{M}^{(k+1)} & \omega \mathbf{H} \end{pmatrix} \begin{pmatrix} \mathbf{y}^{(k+1)} \\ \mathbf{u}^{(k+1)} \end{pmatrix} = \begin{pmatrix} \mathbf{F}^{(k+1)} \\ \mathbf{G}^{(k+1)} \end{pmatrix}.$$

  Update $\lambda^{(k+1)} = \max\{0, \lambda^{(k)} + \eta(y^{(k+1)} - z)\}$;
  $k \leftarrow k + 1$;
until $\mathcal{N}^{(k+1)} = \mathcal{N}^{(k)}$ *or* $k \geq K_{\max}$;
return $y^* = y^{(k+1)}$, $u^* = u^{(k+1)}$, $\lambda^* = \lambda^{(k+1)}$.

The initial guess for starting algorithm can be obtained by solving unconstrained optimal control problem min $\mathcal{F}[y,u]$ subject to $\delta y = u + f$ for $(y^{(0)}, u^{(0)})$ and choosing $\lambda^{(0)} = \max\{0, \Delta y^{(0)} + u^{(0)} + f\}$. This provides a physically meaningful starting point.

Moreover, the stopping criterion $\mathcal{N}^{(k+1)} = \mathcal{N}^{(k)}$ indicates that the inactive point set remains unchanged between two successive iterations. We should note that the convergence behavior of the algorithm depends on the satisfaction of strict complementarity conditions. In fact, if strict complementarity conditions hold in the problem, then the algorithm will reach the desired stopping condition in a finite number of steps, and the obtained solution is the optimal solution [16]. However, if this condition does not hold, the algorithm will enter a loop after a few steps; in this case, we stop the algorithm and accept the resulting solution as a near-optimal solution [14].

5. Numerical illustrations

This section is devoted to the numerical solution of some test cases for the optimal control problem governed by an elliptic variational inequality, as formulated in (P). The simulations employ the IEFG method described in the previous section.

For the radial weight function defined in (3.7), the support radius r is selected proportionally to the fill distance h. The fill distance is given by: $h = \sup_{\mathbf{x}\in\Omega} \min_{\mathbf{x}_i\in\Xi} \|\mathbf{x}_i - \mathbf{x}\|_2$. Specifically, we set $r = \beta h$ with β in the range of 2 to 3 [13].

All computations of this section were performed using MATLAB on a desktop computer equipped with a 3.2 GHz Intel Core i5 processor and 8 GB of RAM.

Example 5.1. In the first example, to validate the proposed numerical framework, a standard benchmark with a known analytical solution is analyzed. The problem is an instance of the variational inequality-constrained optimal control formulation (P), set on the square domain $\Omega = [-1,1]^2$.

The prescribed data for this benchmark are constructed to yield a tractable closed-form solution. The desired state function is as follows

$$y_d(x_1,x_2) = \begin{cases} 200x_1x_2(x_1-0.5)^2(1-x_2), & 0 < x_1 \le 0.5, \\ 200x_2(x_1-1)(x_1-0.5)^2(1-x_2), & 0.5 < x_1 \le 1, \end{cases}$$

and the source term g is defined piecewise along the coordinate x_1:

$$g(x_1,x_2) = \begin{cases} 400\big(x_1(x_1-0.5)^2 - x_2(3x_1-1)(1-x_2)\big), & 0 < x_1 \le 0.5, \\ -200(x_1-0.5), & 0.5 < x_1 \le 1. \end{cases}$$

In this case, the obstacle is set to $z(x_1,x_2) = 0$, and the control regularization parameter is $\omega = 100$.

One can verify by direct substitution that the pair (y^*, u^*) with $u^* \equiv 0$ and

$$y^*(x_1,x_2) = \begin{cases} y_d(x_1,x_2), & 0 < x_1 \le 0.5, \\ 0, & 0.5 < x_1 \le 1, \end{cases}$$

satisfies the first-order optimality system. Consequently, this pair constitutes the unique minimizer, and the corresponding optimal cost evaluates to $\mathcal{F}^* = 25/504$.

Table 1 presents the L_2-norm errors associated with the numerically computed optimal state and control functions on irregular mesh across varying nodal spacing h, using a scaling factor of $\beta = 2.5$ for the support radius. The corresponding absolute error in the approximated objective functional value is also included. To generate the scattered points, we perturb a uniform $n \times n$ Cartesian grid on the unit square $[0,1]^2$ by adding a small random displacement to the interior points, while keeping the boundary points fixed. The perturbation magnitude is controlled by a parameter ϵ, defined relative to the grid spacing h. Specifically, for each interior point, we add independent random perturbations $\delta_k \sim \mathcal{U}(-\epsilon h, \epsilon h)$ for $k = 1, 2$, and clip the resulting points to remain within $[0,1]^2$. This yields a set of n^2 slightly irregular points. In our experiments, we set $\epsilon = 0.15$.To further illustrate the point distribution, Figure 1 shows the considered scattered points for $h = 0.05$ ($n = 400$). The numerical results demonstrate that the proposed method successfully handles such irregular configurations, highlighting its effectiveness beyond structured grids.

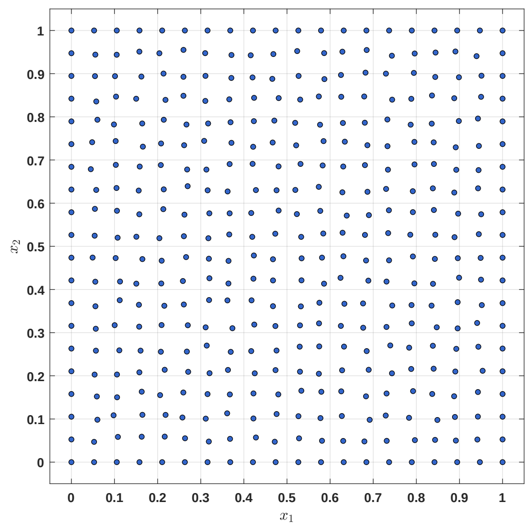

FIGURE 1. The used scattered points on $[0, 1]^2$ for $h = 0.05$ and $\epsilon = 0.15$.

The empirical convergence rate, reflecting the method's order of accuracy, is computed using the formula:

$$\text{Order} = \frac{\log(E^{(h_1)}) - \log(E^{(h_2)})}{\log(h_1) - \log(h_2)},$$

where $E^{(h_1)}$ and $E^{(h_2)}$ denote the numerical errors obtained for the discretization parameters h_1 and h_2, respectively.

Also, Figure 2 shows the obtained optimal state and control functions for $h = 0.01$ with regular grid in the domain. The free boundary separating the active and inactive sets is precisely located at $x_1 = 0.5$. Since the node distribution is structured and the interface aligns exactly with the grid line $x_1 = 0.5$, the presented numerical solution captures the kink in the state function and the jump in its normal derivative across this interface accurately. This confirms the ability of the IEFG method to resolve the free boundary with high precision when the interface is aligned with the discretization.

TABLE 1. The computational order of error for Example 5.1.

	state		*control*		*objective functional*	
h	L_2 error	*order*	L_2 error	*order*	absolute error	*order*
0.2	2.8436e-02	–	1.0629e-02	–	2.5410e-02	–
0.1	8.1520e-03	1.8025	3.0277e-03	1.8117	6.9467e-03	1.8710
0.05	2.2254e-03	1.8731	8.2882e-04	1.8691	1.8737e-03	1.8904
0.02	3.9231e-04	1.8942	1.4598e-04	1.8952	3.2638e-04	1.9073
0.01	1.0466e-04	1.9062	3.8647e-05	1.9173	8.5918e-05	1.9255

The observed convergence rates of approximately 1.8–1.9 are slightly lower than the ideal rate of 2.0 for quadratic IMLS basis functions. This reduction is due to the limited global regularity of the solution caused by the presence of the free boundary (the interface between the active and inactive sets). At this interface, the solution is continuous but its derivative has a jump. Consequently, the solution belongs to the fractional Sobolev space $H^{3/2-\epsilon}(\Omega)$ for any $\epsilon > 0$,

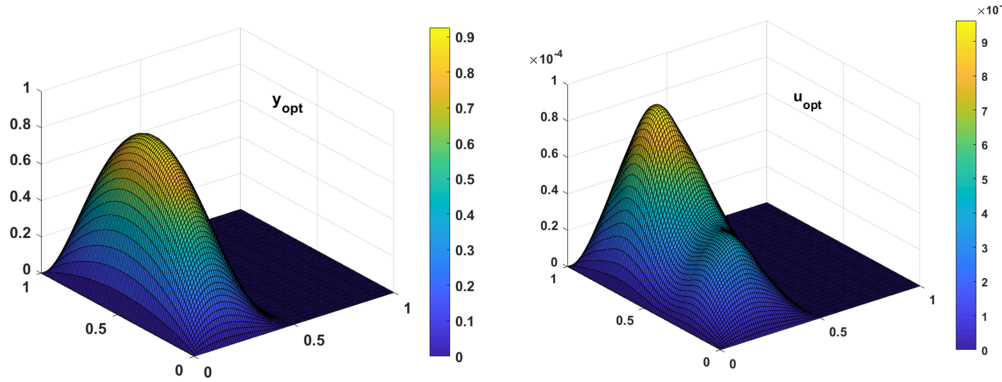

FIGURE 2. Optimal state function (left) and optimal control function (right) for Example 5.1. The obtained free boundary at $x_1 = 0.5$, is in complete agreement with the analytical solution.

but not to $H^2(\Omega)$ nor even $H^{3/2}(\Omega)$. This loss of regularity is a classical result in the theory of obstacle problems (see, e.g., [21]). Standard approximation theory predicts a convergence rate of $O(h^{\min(p+1,s)})$ for functions with regularity H^s, where p is the polynomial degree. With $p = 2$ and $s \approx 1.5$, the theoretical expected rate is $O(h^{1.5})$, The observed convergence rate is therefore consistent with the theoretical expectation and, in fact, exceeds the worst-case bound of $O(h^{3/2-\epsilon})$, confirming the effectiveness of the IEFG method.

Moreover, we compare the proposed IEFG method with two of our previously published numerical methods for the same class of optimal control problems, namely the wavelet collocation method [20] and the pseudo-spectral method [18]. Table 2 summarizes the results for the same discretization parameter, $N = 40$ nodes in each dimension, for all three methods. In general, the pseudo-spectral method achieves the highest accuracy, but it requires a structured grid. The wavelet method offers comparable accuracy with lower CPU time but is more complex to implement, especially for irregular domains. In contrast, the IEFG method provides a good balance: competitive accuracy, moderate computational cost, and flexibility for complex geometries and irregular meshes.

TABLE 2. Comparison of IEFG method with wavelet collocation [20] and pseudo-spectral [18] methods for Example 5.1.

Method	State L_2 error	CPU time (s)	Available for irregular mesh & domain
Pseudo-spectral (2017)	$8.21e{-}7$	45	No
Wavelet collocation (2018)	$6.17e{-}6$	23	No
IEFG (present)	$1.25e{-}4$	12	Yes

Example 5.2. The second test case involves solving the two-dimensional elliptic variational inequality-constrained optimal control problem (P) on the computational domain $\Omega = [0, 1]^2$. The data for this problem are defined by the affine desired state $y_d(x_1, x_2) = 5x_1 + x_2 - 1$, the quadratic obstacle function $z(x_1, x_2) = 4\big(x_1(x_1-1) + x_2(x_2-1)\big) + 1.5$, and a constant source term $g(x_1, x_2) = 0.1$. The regularization coefficient in the cost functional is set to $\omega = 0.1$.

The numerical approximations for the optimal state and control functions computed using the IEFG method with a nodal spacing of $h = 0.05$ are shown in Figure 2. The state function is zero on the boundary (due to homogeneous Dirichlet conditions) and rises in the interior, remaining below the quadratic obstacle $z(x_1, x_2)$. The control function is non-zero only in the inactive region.

Furthermore, the corresponding Lagrange multiplier field $\lambda(\mathbf{x})$ is visualized in Figure 2. The spatial distribution of λ effectively identifies the active set (where $\lambda > 0$ and $y = z$) and the inactive set (where $\lambda = 0$ and $y < z$),

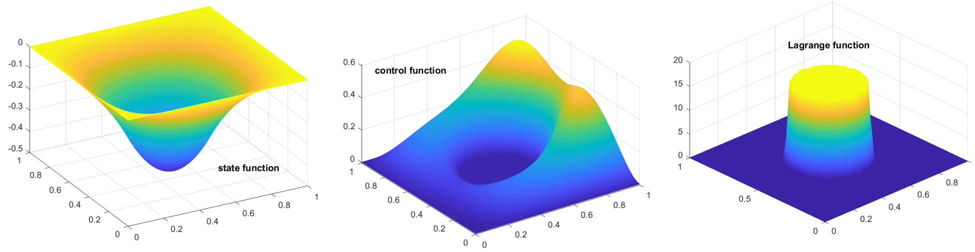

FIGURE 3. The state, control and Lagrangian functions for Example 5.2.

TABLE 3. Convergence of the obtained objective functional values for Example 5.2.

h	$\mathcal{F}[y^*, u^*]$	approximated error	iterations	CPU time(s)	active nodes ratio
0.10	3.38762	$5.187e-03$	5	3.71	0.212
0.05	3.39166	$1.153e-03$	7	3.12	0.173
0.02	3.39253	$2.407e-04$	12	6.23	0.159
0.01	3.39278	$3.118e-05$	21	25.41	0.145

demonstrating the capability of the IEFG formulation to accurately resolve the contact dynamics inherent in the variational inequality.

Table 3 reports the obtained values for $\mathcal{F}[y, u]$ along with the number of iterations of the algorithm to solve the problem on the regular mesh with different values of h. Since an exact solution is not available, the solution obtained from solving the problem with the finite element method with $N = 100^2$ reported in [14] is considered as the reference solution and the the approximated error of the IEFG method is reported. Also, in this table, the ratio of nodes that are in the active region to the total number of nodes is reported.

6. Conclusion

This paper developed a meshless computational framework for solving elliptic variational inequality-constrained optimal control problems. The proposed methodology utilizes interpolating moving least squares (IMLS) shape functions to construct an interpolating element-free Galerkin (IEFG) formulation. The first-order optimality system for the control problem was derived via a regularization technique, and an iterative active-set algorithm was introduced for its numerical solution.

The numerical experiments include two test cases. For the first example, the convergence rates of approximately 1.8–1.9 are observed, which is consistent with the reduced regularity of the solution at the free boundary. The second example demonstrates the applicability of the method to problems without an analytical solution. A comparison with our previously published wavelet collocation and pseudo-spectral methods shows that the IEFG approach offers competitive accuracy while providing greater geometric flexibility, especially for irregular domains. The obtained results confirm that the IEFG-based approach is computationally efficient and yields accurate approximations for this class of nonlinear optimal control problems governed by variational inequalities.

Future work will focus on extending the proposed IEFG method to optimal control problems governed by time-dependent variational inequalities, where the active set evolves over time and requires efficient tracking strategies. Moreover, the extension to three-dimensional problems is another important direction, particularly for realistic engineering applications such as contact mechanics and optimal design in complex geometries. In such cases, the meshless nature of IEFG is expected to offer significant advantages over conventional grid-based methods.

References

[1] M. Abbaszadeh and M. Dehghan, *Numerical and analytical investigations for solving the inverse tempered fractional diffusion equation via interpolating element-free galerkin (IEFG) method.*, Journal of Thermal Analysis & Calorimetry, *143* (2021).

[2] M. Abbaszadeh, M. Dehghan, A. Khodadadian, and C. Heitzinger, *Analysis and application of the interpolating element free galerkin (IEFG) method to simulate the prevention of groundwater contamination with application in fluid flow*, Journal of Computational and Applied Mathematics, *368* (2020), 112453.

[3] O. Abu Arqub and N. Shawagfeh, *Solving optimal control problems of fredholm constraint optimality via the reproducing kernel Hilbert space method with error estimates and convergence analysis*, Mathematical Methods in the Applied Sciences, *44* (2021), 7915–7932.

[4] A. Awad Nasser, M. Allame, H. Abed Kadhim Aal-Rkhais, and M. Tavassoli Kajani, *Application of the meshless interpolating element-free galerkin method for the numerical solution of obstacle problem*, Computational Methods for Differential Equations, (2025), In press.

[5] V. Barbu and G. da Prato, *Optimal control of variational inequalities*, vol. 100, Pitman Boston, 1984.

[6] T. Belytschko, Y. Y. Lu, and L. Gu, *Element-free galerkin methods*, International journal for numerical methods in engineering, *37* (1994), 229–256.

[7] F. Ben Belgacem and Y. Renard, *Hybrid finite element methods for the signorini problem*, Mathematics of Computation, *72* (2003), 1117–1145.

[8] Y. Cheng, J. Wang, and X. Li, *Improved interpolating moving least squares method*, Applied Mathematics and Computation, *420* (2022), 126895.

[9] M. Dehghan and D. Mirzaei, *Radial basis function methods for optimal control of pdes*, Applied Numerical Mathematics, *198* (2024), 234–258.

[10] N. Goudarzian, H. Hassani, and M. S. Dahaghin, *Optimal solution of the nonlinear time fractional diffusion-wave equation using generalized Laguerre polynomials*, Computational Methods for Differential Equations, (2025), In press.

[11] C. Grossmann, H. G. Roos, and M. Stynes, *Numerical treatment of partial differential equations*, Springer, 2007.

[12] M. Hintermüller and A. Laurain, *Optimal shape design subject to elliptic variational inequalities*, SIAM journal on control and optimization, *49* (2011), 1015–1047.

[13] M. Ilati, *Analysis and application of the interpolating element-free galerkin method for extended Fisher–Kolmogorov equation which arises in brain tumor dynamics modeling*, Numerical Algorithms, *85* (2020), 485–502.

[14] K. Ito and K. Kunisch, *Optimal control of elliptic variational inequalities*, Applied Mathematics and Optimization, *41* (2000), 343–364.

[15] K. Ito and K. Kunisch, *Active-set strategies for optimal control of variational inequalities*, Optimal Control Applications and Methods, *46* (2025), 1–18.

[16] T. Kärkkäinen, K. Kunisch, and P. Tarvainen, *Augmented lagrangian active set methods for obstacle problems*, Journal of Optimization Theory and Applications, *119* (2003), 499–533.

[17] M. Khaksar-e Oshagh, M. Abbaszadeh, E. Babolian, and H. Pourbashash, *An adaptive wavelet collocation method for the optimal heat source problem*, International Journal of Numerical Methods for Heat & Fluid Flow, *32* (2022), 2360–2382.

[18] M. Khaksar-e Oshagh and M. Shamsi, *Direct pseudo-spectral method for optimal control of obstacle problem–an optimal control problem governed by elliptic variational inequality*, Mathematical Methods in the Applied Sciences, *40* (2017), 4993–5004.

[19] M. Khaksar-e Oshagh and M. Shamsi, *An adaptive wavelet collocation method for solving optimal control of elliptic variational inequalities of the obstacle type*, Computers & Mathematics with Applications, *75* (2018), 470–485.

[20] M. Khaksar-e Oshagh, M. Shamsi, and M. Dehghan, *A wavelet-based adaptive mesh refinement method for the obstacle problem*, Engineering with Computers, *34* (2018), 577–589.

[21] D. Kinderlehrer and G. Stampacchia, *An Introduction to Variational Inequalities and Their Applications*, no. 31 in Classics in Applied Mathematics, Society for Industrial and Applied Mathematics (SIAM), Philadelphia, PA, 2000.

[22] M. Lakestani and R. Tuntaş, *Efficient solution for multi-delay fractional optimal control problems via cubic b-splines*, Optimal Control Applications and Methods, *46* (2025), 2411–2422.

[23] M. Lakestani, R. Tuntaş, and M. Dehghan, *Constructing efficient bases from b-spline functions and solving fractional optimal control problems*, Journal of Applied Mathematics and Computing, *72* (2026), 120.

[24] X. Li, H. Chen, and Y. Wang, *Error analysis in Sobolev spaces for the improved moving least-square approximation and the improved element-free galerkin method*, Applied Mathematics and Computation, *262* (2015), 56–78.

[25] D. Liu and Y. Cheng, *The interpolating element-free galerkin (IEFG) method for three-dimensional potential problems*, Engineering Analysis with Boundary Elements, *108* (2019), 115–123.

[26] D. Mirzaei and M. Dehghan, *Meshfree methods for optimal control problems: a review*, Engineering Analysis with Boundary Elements, *152* (2023), 123–145.

[27] S. Niknam and H. Adibi, *A numerical solution of two-dimensional hyperbolic telegraph equation based on moving least square meshless method and radial basis functions*, Computational Methods for Differential Equations, *10* (2022), 969–985.

[28] H. Pourbashash, M. Khaksar-e Oshagh, S. Asadollahi, et al., *An efficient adaptive wavelet method for pricing time-fractional american option variational inequality*, Computational Methods for Differential Equations, *12* (2024), 173–188.

[29] F. Samadi, *Enhancing the Legendre-Gauss-Radau pseudospectral method with sigmoid-based control parameterization for solving bang-bang optimal control problems*, Computational Methods for Differential Equations, *13* (2025), 802–814.

[30] F. Sun, J. Wang, Y. Cheng, and A. Huang, *Error estimates for the interpolating moving least-squares method in n-dimensional space*, Applied Numerical Mathematics, *98* (2015), 79–105.

[31] L. Zhang, Y. Wang, and H. Chen, *A comparative study of meshfree methods for optimal control problems*, Journal of Applied Mathematics and Computing, *71* (2025), 1–25.